ACCOUNTS of chemical research

Article

Cite This: Acc. Chem. Res. 2018, 51, 2793−2802

pubs.acs.org/accounts

Insights into Interfaces, Stability, Electronic Properties, and Catalytic Activities of Atomically Precise Metal Nanoclusters from First Principles

Published as part of the Accounts of Chemical Research special issue "Toward Atomic Precision in Nanoscience".

Qing Tang,[†] Guoxiang Hu,[‡] Victor Fung,[‡] and De-en Jiang*[,‡]

[†]School of Chemistry and Chemical Engineering, Chongqing University, Chongqing 401331, China

[‡]Department of Chemistry, University of California, Riverside, California 92521, United States

CONSPECTUS: Atomically precise, ligand-protected metal nanoclusters are of great interest for their well-defined structures, intriguing physicochemical properties, and potential applications in catalysis, biology, and nanotechnology. Their structure precision provides many opportunities to correlate their geometries, stability, electronic properties, and catalytic activities by closely integrating theory and experiment. In this Account, we highlight recent theoretical advances from our efforts to understand the metal−ligand interfaces, the energy landscape, the electronic structure and optical absorption, and the catalytic applications of atomically precise metal nanoclusters. We mainly focus on gold nanoclusters.

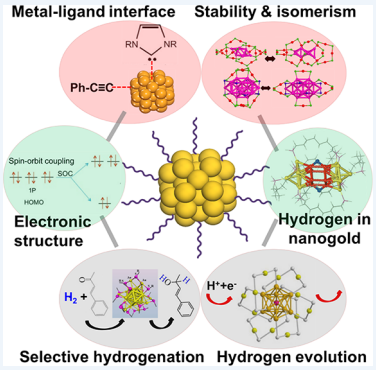

The bonding motifs and energetics at the gold−ligand interfaces are two main interests from a computational perspective. For the gold−thiolate interface, the −RS−Au−SR− staple motif is not always preferred; in fact, the bridging motif (−SR−) is preferred at the more open facets such as Au(100) and Au(110). This finding helps understand the diversity of the gold−thiolate motifs for different core geometries and sizes. A great similarity is demonstrated between gold−thiolate and gold−alkynyl interfaces, regarding formation of the staple-type motifs with PhC≡C− as an example. In addition, N-heterocyclic carbenes (NHCs) without bulky groups also form the staple-type motif. Alkynyls and bulky NHCs have the strongest binding with the gold surface from comparing 27 ligands of six types, suggesting a potential to synthesize NHC-protected gold clusters.

The energy landscape of nanosystems is usually complex, but experimental progress in synthesizing clusters of the same Au−S composition with different R groups and isomers of the same $Au_n(SR)_m$ formula have made detailed theoretical analyses of energetic contributions possible. Ligand−ligand interactions turn out to play an important role in the cluster stability, while metastable isomers can be obtained via kinetic control.

Although the superatom-complex theory is the starting point to understand the electronic structure of atomically precise gold clusters, other factors also greatly affect the orbital levels that manifest themselves in the experimental optical absorption spectra. For example, spin−orbit coupling needs to be included to reproduce the splitting of the HOMO−LUMO transition observed experimentally for $Au_{25}(SR)_{18}^-$, the poster child of the family. In addition, doping can lead to structural changes and charge states that do not follow the superatomic electron count.

Atomically precise metal nanoclusters are an ideal system for understanding nanocatalysis due to their well-defined structures. Active sites and catalytic mechanisms are explored for selective hydrogenation and hydrogen evolution on thiolate-protected gold nanoclusters with and without dopants. The behavior of H in nanogold is analyzed in detail, and the most promising site to attract H is found to be coordinately unsaturated Au atoms.

Many insights have been gained from first-principles studies of atomically precise, ligand-protected gold nanoclusters. Interesting and important questions remaining to be addressed are pointed out in the end.

1. INTRODUCTION

During the past decade, great advances have been made in synthesis, crystallization, and structure determination of atomically precise Au, Ag, Cu, bimetallic, and multimetallic nanoclusters with tens to hundreds of metal atoms protected by ligands such as thiolates, alkynyls, phosphines, and hydrides.[1−3] Their well-defined structures allow theory and computation to provide important insights into their structure−property and structure−function relationships.

Ligands play a critical role in determining the structures, stability, and properties of metal nanoclusters. They are important not only for stabilizing the metal cores but also to generate unique and chemically active interfaces for many important applications. Thiols are the most popular ligands for Au nanoclusters, while alkynyls have recently emerged as a new paradigm in yielding new structures.[4] More recently, carbenes have been used to stabilize and functionalize metal surfaces.[5]

Ligand-protected metal nanoclusters exhibit molecular-like electronic behaviors which sharply distinguish them from

Received: July 31, 2018
Published: November 6, 2018

DOI: 10.1021/acs.accounts.8b00380
Acc. Chem. Res. 2018, 51, 2793−2802

metallic nanoparticles. Particularly, in the small size regime (below ~2 nm), the electronic structures and optical absorption spectra depend upon size, composition, and structure, thereby serving as a fingerprint to identify and distinguish ultrasmall nanoclusters in their formation and growth process.[3]

One of the most important applications of atomically precise metal nanoclusters is catalysis.[1] They can be used as homogeneous catalysts in solutions or loaded onto solid supports as heterogeneous catalysts, in thermal catalysis, electrocatalysis, and photocatalysis. They have been used in reactions such as selective hydrogenation, water splitting, and CO_2 reduction.

Due to the well-defined structures and the relatively small sizes of many atomically precise nanoclusters, they are perfect systems for first-principles understandings of many fundamental questions regarding their structure, energetics, interfaces, formation, growth, properties, reactions, and catalytic mechanisms. Density functional theory (DFT) methods have proven very successful in providing insights into those questions. After briefly introducing the DFT approach in the cluster study (section 2), this Account will focus on our recent DFT studies of atomically precise gold nanoclusters, coupled with experiment, in understanding the ligand−metal interfaces; the ligand-dependent stability and isomerism; the effect of spin−orbital coupling and heteroatom doping on the optical absorption and electronic transitions; the catalytic mechanisms.

2. DENSITY FUNCTIONAL THEORY IN CLUSTER RESEARCH

DFT comes in different flavors mainly due to the different levels and choices of treatment of electron exchange-correlation. For structural and energetic accuracies relevant to chemistry, generalized-gradient approximation (GGA) or higher is required. The popular Perdew−Burke−Ernzerhof (PBE) GGA functional has been the de facto choice for structural and energetic studies of atomically precise nanoclusters, due to a well-demonstrated balance of accuracy and computational cost.[6] DFT-PBE's famous successes include structure prediction for $Au_{25}(SR)_{18}$ and $Au_{38}(SR)_{24}$ that were confirmed by experiment.[6,7] In terms of the interaction between electrons and the nuclei, the effective core potentials or pseudopotentials including the scalar relativistic effects are routinely employed for cluster systems with heavy metals such as Au. DFT also contributed significantly to the understanding of the cluster stabilities and electronic structures of $Au_n(SR)_m$ from the "superatom" concept.[8] Moreover, the time-dependent DFT (TDDFT) calculations with GGA or hybrid functionals yield optical absorption spectra in good agreement with experiment; they are often employed to study the orbital symmetry/splitting and the structure-optical absorption correlation of pristine or doped small-size nanoclusters.[1] In addition, DFT has also been used to predict circular dichroism (CD) spectra, ligand-exchange reactions, and photoemission core-level shifts of $Au_n(SR)_m$ nanoclusters.[6] Last but not least, DFT coupled with transition state search methods is the most important tool to understand the catalytic mechanism on atomically precise metal nanoclusters from first principles. Below we will discuss the insights from DFT into interfaces, electronic and optical properties, and catalytic activities of atomically precise metal nanoclusters, drawing mainly from our own work but also putting them into the perspective of the field.

3. INTERFACES

Without a doubt, the metal−ligand interface is the most interesting part of the geometry of an atomically precise metal nanocluster. To reveal the driving force for the interface formation, the first-principles energetics from DFT, which is a total-energy method after all, provides the most valuable information. We were particularly intrigued by the comparison of different motifs and different ligands at the interfaces, so we will first discuss the popular gold−thiolate interface and then the emerging ligands.

The Gold−Thiolate Interface: Staple vs Bridging

Since their discovery on the Au(111) surface in 2006[9] and in the $Au_{102}(SR)_{44}$ cluster in 2007,[10] the staple motifs (namely, the $-SR-[Au-SR-]_x$ oligomers for x = 1, 2, etc.) have been thought as the key feature of the gold−thiolate interface and a leading hypothesis for the structure prediction of $Au_n(SR)_m$ nanoclusters.[7] The staple hypothesis, however, has been challenged by the recently solved structure of $Au_{92}(SPh\text{-}p\text{-}^tBu)_{44}$,[11] which also has bridging thiolates (−SR−) at the interface. This finding demanded a rethinking of the gold−thiolate interface and raised the question about the surface sensitivity of different bonding motifs. To answer this question, we compared the energetic stability of the staple vs bridging mode of thiolates at different low-Miller-index surfaces of gold (Figure 1a,b) using DFT-PBE.[12] Interestingly, the staple motif was found to be energetically preferred on Au(111), but the bridging motif is preferred on Au(100) and Au(110). This surface-sensitive trend can be understood by the decreasing coordination number of the surface Au atom from Au(111) to Au(100) to Au(110): the lower the coordination, the higher reactivity and stronger binding with the ligand; more so for the bridging thiolate than for the thiolate in the staple motif, leading to a reversal of the relative stability.

The surface sensitivity could explain the different surface-protecting modes observed in $Au_n(SR)_m$. The $Au_n(SR)_m$ structures can be divided into three groups (Figure 1c): (1) no bridging, e.g., $Au_{25}(SR)_{18}^-$, $Au_{38}(SR)_{24}$; (2) ambiguous bridging, e.g., $Au_{36}(SR)_{24}$, $Au_{44}(SR)_{28}$; (3) distinct bridging, e.g., $Au_{92}(SR)_{44}$. The "no bridging" clusters usually have nonfcc cores (e.g., icosahedral, hcp), and the core surfaces usually comprise the interconnected Au_3 triangles, reminiscent of the Au(111) facets which prefers the staple motif (Figure 1b). In contrast, clusters belonging to ambiguous or distinct bridging type have fcc cores that tend to expose Au_4 squares, resembling the (100) facets where the bridging motif is slightly preferred (Figure 1b). Interestingly, the bridging thiolates in the "ambiguous" type can be viewed alternatively as part of the distorted staple motifs with a different core geometry. Taking $Au_{36}(SR)_{24}$ as an example (Figure 1c, middle), it can be viewed as an fcc Au_{28} kernel (magenta) protected by 4 dimeric staples (green) and 12 bridging motifs (blue); alternatively, the 12 bridging motifs together with the 8 kernel Au atoms between them can be viewed as 4 additional "distorted" dimeric staples protecting a Au_{20} kernel. The bridging-motif view and the staple-motif view in the case of "ambiguous bridging" offer us a more complete understanding of the gold−thiolate interface, as the two sides of the same coin.

Emerging Ligands: Alkynyl

Besides the widely used thiolates, alkynyls and carbenes have recently emerged as new paradigm of ligands to protect gold. For alkynyls, Tsukuda et al.[13] first introduced phenylacetylene as the stabilizer and synthesized a series of alkynyl-protected

DOI: 10.1021/acs.accounts.8b00380
Acc. Chem. Res. 2018, 51, 2793−2802

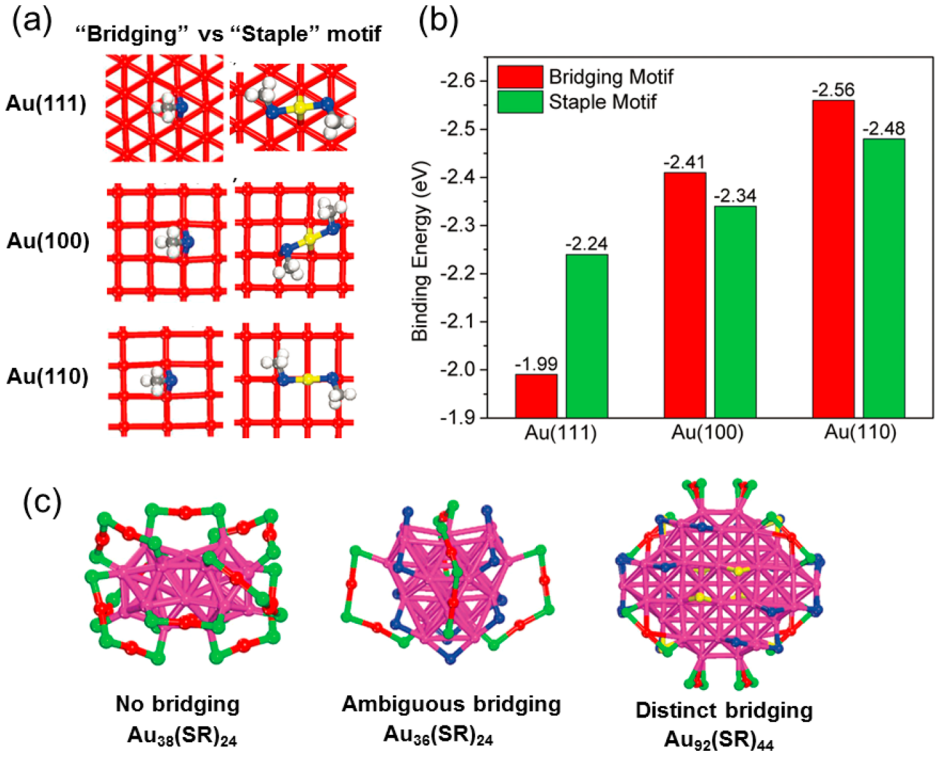

Figure 1. (a) Bridging and staple motifs of methylthiolate (CH_3S-) on Au(111), Au(100), and Au(110) (top view). Au_{adatom}, yellow; other Au, red. (b) Comparison of binding energies per methylthiolate for the bridging vs staple motifs on the three Au surfaces. (c) Three types of $Au_n(SR)_m$ clusters. Au (core), magenta; Au (staple), red; S (staple), green; S (ambiguous bridging), blue; S (distinct bridging), yellow. Adapted with permission from ref 12. Copyright 2016 Royal Society of Chemistry.

clusters, but their structures were unknown. Very interestingly, our DFT-PBE studies on PhC≡C−/Au(111) and PhC≡C−/Au_{20} interfaces predicted that PhC≡C− forms similar staple motifs as the thiolates.[14] Yet PhC≡C− has a different coordination preference due to π-bonding with the Au surface. Figure 2a shows that if we start with one Au adatom and two isolated PhC≡C− on Au(111), formation of the PhCC−Au_{adatom}−CCPh motif would lower the energy significantly by ∼1.58 eV, indicating the favorable thermodynamics for π bonding of C≡C with the surface gold in addition to the PhCC−Au σ bonds in the motif. At the PhCC/Au_{20} interface, both the monomeric [PhCC−Au−CCPh] and dimeric [PhCC−Au−CCPh−Au−CCPh] staple motifs (Figure 2b) were found at the interface from our DFT-based first-principles molecular dynamics simulations, in close analogy to thiolates on Au.

Impressive synthesis advances have been made by the Wang[4] and Zheng[15,16] groups in the crystallization of alkynyl-protected gold nanoclusters. Their total-structure determinations confirmed the presence of the π-bonding staple motifs at the interface. Importantly, the [PhCC−Au−CCPh] motif observed in $Au_{24}Ag_{20}$,[16] $Au_{34}Ag_{28}$,[15] and $Au_{80}Ag_{30}$,[4] and the [PhCC−Au−CCPh-Au−CCPh] motif observed in Au_{19}, Au_{23},[4] Au_{36}, and Au_{44}[17] are exactly as our predictions using DFT-PBE (Figure 2b).[14] More interestingly, $Au_{36}(PhC{\equiv}C)_{24}$ and $Au_{44}(PhC{\equiv}C)_{28}$[17] closely resemble $Au_{36}(SR)_{24}$ and $Au_{44}(SR)_{28}$, respectively, in structure, suggesting a parallel universe between Au−thiolate and Au−alkynyl nanoclusters. Encouragingly, the recently solved structure of $Au_{144}(C{\equiv}C{-}Ar)_{60}$[18] matches the best model proposed for $Au_{144}(SR)_{60}$ whose total-structure determination has been unsuccessful despite years of effort.

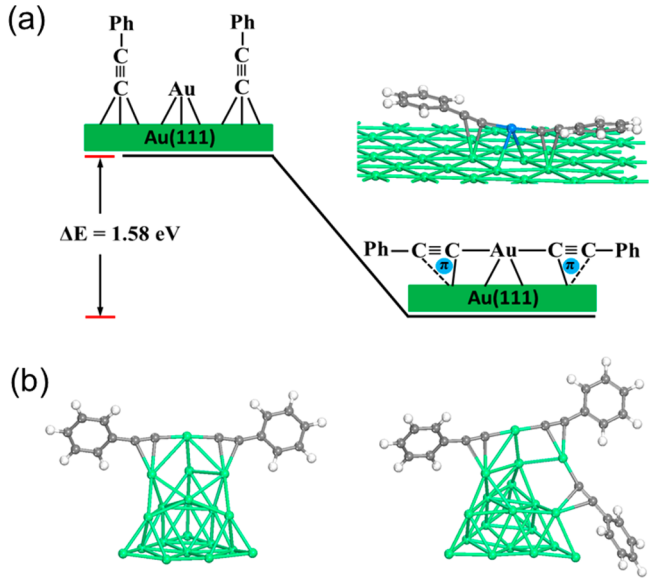

Figure 2. (a) Energy of the π-bonding PhCC−Au−CCPh staple motif relative to isolated Au adatom and PhC≡C− on Au(111). (b) Monomeric and dimeric staple motifs of PhC≡C− on Au_{20}. Adapted with permission from ref 14. Copyright 2015 American Chemical Society.

Emerging Ligands: *N*-Heterocyclic Carbenes (NHCs)

NHCs are well-established ligands for metal complexes.[5] Recently, researchers began to explore self-assembled monolayersof NHCs on surfaces. The NHC monolayers on Au display high stability under harsh conditions.[19] Wang et al. reported the formation of NHC−gold adatom complex by

DOI: 10.1021/acs.accounts.8b00380
Acc. Chem. Res. 2018, 51, 2793−2802

scanning tunneling microscopy (STM)[20] and assumed that the carbene−metal bond perpendicular to the metal surface. Using DFT-PBE, we found that the presence of gold adatoms greatly enhances the binding strengths of NHC to gold.[21] Particularly, substituents at the *N*,*N*-positions of NHC are critical in determining the binding modes. Small NHCs with methyl substitutes prefer to pair via the adatom and form a flat-lying NHC−Au_{adatom}−NHC motif (Figure 3a), analogous to the staple motif with thiolates, while bulky NHCs with 2,4,6-trimethylphenyl substitutes sterically hinder the dimerization of carbenes and adopt the upright fashion only (Figure 3b). Indeed, the recent STM study by Papageorgiou et al.[22] verified that the NHC−metal−NHC dimeric motif is the general bonding pattern of small NHCs to coinage metal surfaces. Independently, Crudden et al.[23] observed flat NHC−metal-NHC dimeric motif for methyl-(ethyl)-substituted NHCs and upstanding NHC−adatom complex for isopropyl-substituted NHCs, confirming our prediction.

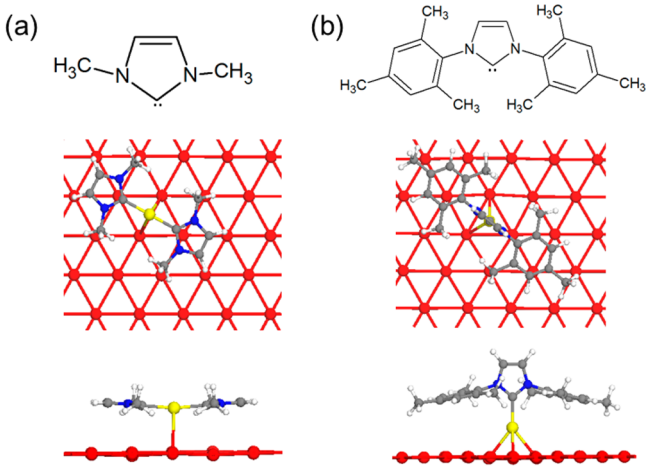

Figure 3. Bonding-geometry comparison of a simple NHC (a) and a bulky NHC (b) on Au-adatom(yellow)-decorated Au(111). Adapted with permission from ref 21. Copyright 2017 American Chemical Society.

Comprehensive Comparison of the Gold−Ligand Interfacial Energetics

Given the increasing number of ligands developed for protecting metal surfaces, it is necessary to compare their interface stability. We selected 27 ligands of six different types (Figure 4a) and investigated their interaction with the model Au(111) surface by dispersion-corrected DFT.[21] Among them, bulky NHCs and alkynyl groups exhibit the strongest binding (Figure 4b). The stronger binding of bulky NHCs than the less steric NHCs to Au mainly arises from the van der Waals (vdW) contribution of bulky side groups with surface via the short Au···HCH_2R contact. The remarkable stability of gold-alkynyl and gold-NHC interfaces hinted that they may outperform thiolates and phosphines to yield more stable metal nanoclusters. In fact, we have designed a few such clusters for NHCs with the free-electron count of eight.[21]

4. ROLE OF LIGANDS IN CLUSTER STABILITY AND ISOMERISM

The preceding discussion revealed that different ligands will lead to different interfacial structures and energetics. This section focuses on the role of the ligands in dictating the stability of the whole cluster, another question for which DFT total energies are extremely useful. Especially, we are interested in how the ligands dictate the relative stability of clusters or the energy landscape of the same composition. Synthetic advances have provided a few examples for theory to shed some light on this question. The first example is $Au_{24}(SR)_{20}$ (Figure 5a) for which there are two competing models: one predicted by Pei et al.,[24] comprising a prolate Au_8 core capped by interlocked trimeric and pentameric staples ("P" model); an experimentally determined one featuring an antiprismatic Au_8 core protected by tetrameric staples for R = CH_2Ph−^{t}Bu ("J" model).[25] The two different models for the same $Au_{24}(SR)_{20}$ formula begged the question: would the cluster of the same Au−S composition adopt a different structure as R changes? We found that the answer is yes. By comparing the relative energies at the DFT-PBE-D3 level,[26] we found that when R = $-C_2H_4Ph$, P isomer is more stable by 1.6 eV due to the stronger vdW interactions among the $-C_2H_4Ph$ tail groups, while for

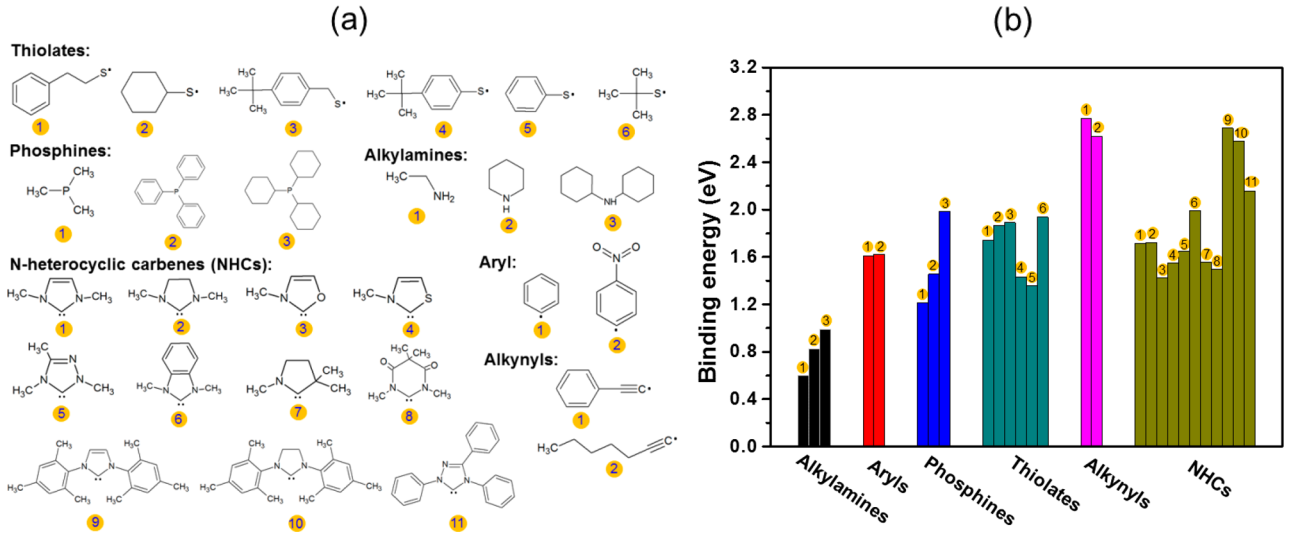

Figure 4. (a) 27 ligands of six different types compared for protecting gold surface. (b) Binding energies of the 27 ligands on Au_{adatom}−Au(111) at the DFT-PBE-D3 level with scaling; the number sequence in each type of ligands matches the ligand structures in (a) for that type. Adapted with permission from ref 21. Copyright 2017 American Chemical Society.

DOI: 10.1021/acs.accounts.8b00380
Acc. Chem. Res. 2018, 51, 2793−2802

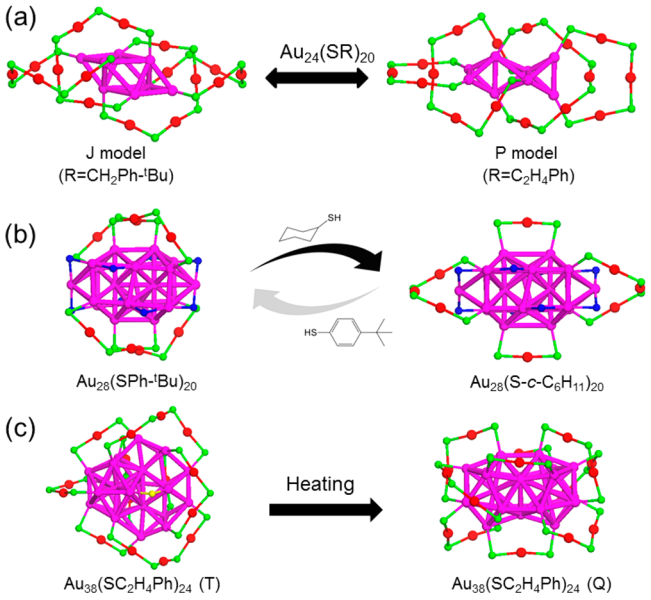

Figure 5. R-group-dependent structural change of the same Au−S composition in $Au_{24}(SR)_{20}$ (a) and $Au_{28}(SR)_{20}$ (b). Isomerism in $Au_{38}(SC_2H_4Ph)_{24}$ (c). Only the Au−S framework is shown; Au (core), magenta; Au (staple), red; S (staple), green; S (ambiguous bridging), blue; S (distinct bridging), yellow.

R = $-CH_2Ph$-^{t}Bu, J isomer is more stable by 1.0 eV, due to its better capacity to accommodate the steric effect of bulkier $-CH_2Ph$-^{t}Bu groups. This reversal of stability suggests the critical role of ligands in dictating the isomer stability.

Another interesting example was revealed recently by Jin and Jiang.[27] $Au_{28}(SPh\text{-}^tBu)_{20}$ was prepared and reacted with excess cyclohexanethiol to yield $Au_{28}(S\text{-}c\text{-}C_6H_{11})_{20}$. The two clusters have the same rod-shaped Au_{20} kernel, but the arrangements of the protecting motifs are different (Figure 5b). DFT calculations found that the experimental structure is indeed the more stable form of that ligand.[27] In other words, DFT confirmed the changing energy landscape of the same $Au_n(SR)_m$ composition as the R group changes, due to the combined effect of ligand−ligand and ligand-gold interactions.

In addition to the structural change induced by different ligands, Tian et al.[28] reported a "true" structural isomerism in $Au_{38}(SR)_{24}$ with the same $-SC_2H_4Ph$ ligand (Figure 5c). They crystallized a metastable isomer of $Au_{38}(SC_2H_4Ph)_{24}$ (Au_{38T}) via the low-temperature synthesis and kinetic control, as compared to the more stable $Au_{38}(SC_2H_4Ph)_{24}$ reported earlier (Au_{38Q}). Interestingly, the Au_{38T} isomer would transform irreversibly to the ground-state Au_{38Q} when heated.

5. ELECTRONIC STRUCTURE AND OPTICAL ABSORPTION

After discussing the interfaces and stability, it is natural now to look into the electronic structure of these ligand-protected gold nanoclusters. Experimental progress in crystallization and characterization of atomically precise nanoclusters has greatly motivated theoretical studies to elucidate their electronic structures and optical transitions. Take the most popular cluster $Au_{25}(SR)_{18}$ as an example. According to the "superatom" theory,[8] the eight free electrons of $Au_{25}(SR)_{18}^-$ fill up the superatomic orbitals as $(1S)^2(1P)^6$. The 3-fold degenerate HOMO is of P character, while the 2-fold-degenerate LUMO and 3-fold-degenerate LUMO+1 are of D character (Figure 6a). However, this simple orbital-level picture would change as spin−orbit coupling is considered or other metal atoms are doped into the structure.

Spin−Orbit Coupling

The UV−vis absorption spectrum of $Au_{25}(SR)_{18}^-$ measured at room temperature shows a main peak at 1.8 eV with a shoulder at 1.6 eV (Figure 7a top).[30] At lower temperatures,[31] the shoulder evolves into a distinct peak at 1.67 eV, next to the main peak at 1.90 eV (Figure 6b). The previous simulated spectrum of $Au_{25}(SCH_3)_{18}^-$ by TDDFT, however, shows only one peak in this region.[30] To solve this discrepancy, we hypothesized that spin−orbit coupling (SOC) is the reason, so we included SOC in the excited-state calculations.[29] Right away one can see that the one peak in the spectrum without SOC splits into two with SOC (Figure 6c). It turns out that SOC causes splitting of the HOMO 1P orbital into doubly degenerate $1P_{3/2}$ and nondegenerate $1P_{1/2}$, separated by 0.2 eV (Figure 6d). The splitting of the LUMO from SOC is negligible. Accordingly, the transitions from $1P_{3/2}$ and $1P_{1/2}$ to LUMO generate the separated α_1 and α_2 peaks (Figure 6c), respectively. This case highlights the importance of SOC in the electronic structure of gold nanoclusters.

Doping

Doping $Au_{25}(SR)_{18}$ has been fruitfully explored since DFT predicted that the central gold of $Au_{25}(SR)_{18}^-$ can be substituted by many other elements.[33] Negishi et al.[34] and Jin et al.[35] synthesized $PdAu_{24}$ and $PtAu_{24}$. Wu et al.[36] confirmed that Pd and Pd are indeed located at the icosahedral center from X-ray structure determination. Interestingly, as-synthesized $PdAu_{24}$ and $PtAu_{24}$ were charge-neutral, indicating that they prefer the 6-electron $(1S)^2(1P)^4$ electronic configuration (Figure 7b left). The change in the electronic structure is reflected by the dramatic decrease in the electrochemical gap of the doped systems (~0.3 eV) compared to $Au_{25}(SR)_{18}^-$ (1.32 eV).[32] The optical absorption spectrum also changes significantly (Figure 7a): a distinct near-infrared band (α) appeared below 1.5 eV, which was absent in $Au_{25}(SR)_{18}^-$. Our DFT studies showed that the HOMO 1P orbitals split upon Pd(Pt) doping into doubly degenerate HOMO and one LUMO (Figure 7b), resulting in decreased HOMO−LUMO gap.[32] The observed α and γ peaks in Figure 7a correspond to HOMO−1 to LUMO and HOMO to LUMO+1 transition, respectively. The 1P splitting also resulted in a Jahn−Teller-like distortion of the $M@Au_{12}$ core, which became more oblate compared to the spherical-like Au_{13} core (Figure 7b left). Interestingly, the 6-electron $[MAu_{24}(SR)_{18}]^0$ (M = Pd, Pt) could be reversibly reduced to 8-electron $[MAu_{24}(SR)_{18}]^{2-}$ electrochemically. In another study,[37] Lee and Jiang groups investigated doping of Pd and Pt in $Au_{38}(SR)_{24}$; they found $[Pt_2Au_{36}(SR)_{24}]^{2-}$ and $[Pd_2Au_{36}(SC_6H_{13})_{24}]^0$ to be the as-synthesized charge states which relate to the different degrees of structural distortions caused by doping.

6. CATALYTIC MECHANISMS IN SELECTIVE HYDROGENATION AND HYDROGEN EVOLUTION

The well-defined geometry and electronic structure of atomically precise metal nanoclusters offer a chemical basis to understand their many applications, with catalysis being the most prominent one. Previous research mainly focused on thermal catalysis (e.g., oxidation, hydrogenation, C−C coupling), yet recent efforts have demonstrated their great promise for electrocatalysis.[1] The greatest advantage of atomically precise metal nanoclusters as a model catalyst is

DOI: 10.1021/acs.accounts.8b00380
Acc. Chem. Res. 2018, 51, 2793−2802

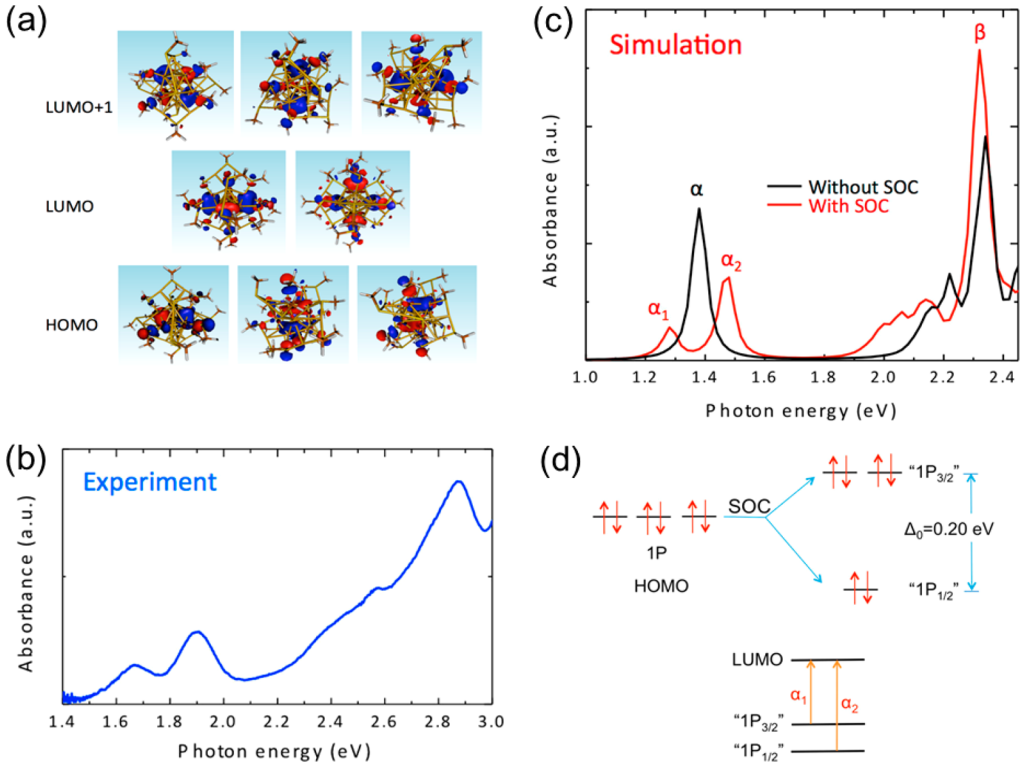

Figure 6. (a) Frontier orbitals of $Au_{25}(SR)_{18}^{-}$. Experimental (b) and simulated (c) optical absorption spectra of $Au_{25}(SR)_{18}^{-}$. (d) Energy diagrams to show splitting of HOMO 1P due to spin−orbit-coupling (SOC) and its effect on optical transition. Adapted with permission from ref 29. Copyright 2014 American Chemical Society.

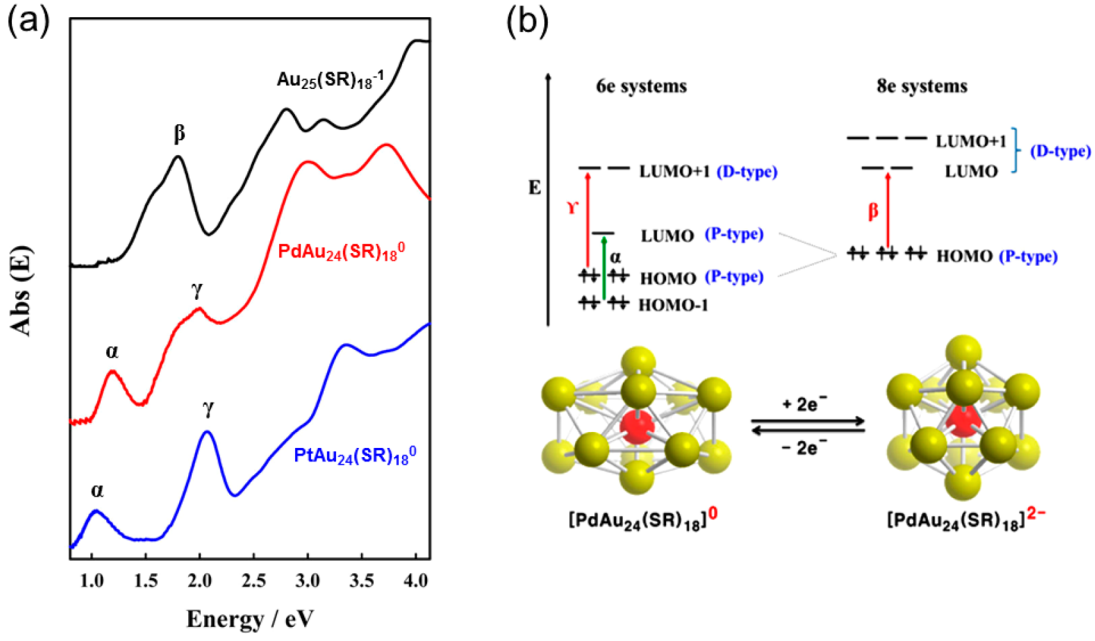

Figure 7. (a) Experimental UV−vis−NIR absorption spectra of $Au_{25}(SR)_{18}^{-}$, $[PdAu_{24}(SR)_{18}]^{0}$, and $[PtAu_{24}(SR)_{18}]^{0}$. (b) Calculated electronic energy levels of 6-electron ($[MAu_{24}(SR)_{18}]^{0}$; M = Pd, Pt) and 8-electron ($[MAu_{24}(SR)_{18}]^{2-}$) systems and the Jahn−Teller distortion in the core. Adapted with permission from ref 32. Copyright 2015 American Chemical Society.

their well-defined structures allowing a thorough DFT modeling of the active sites and the catalytic mechanisms. Below we highlight several examples.

Au_{25} for Selective Hydrogenation

Controlling the selective hydrogenation of α,β-unsaturated ketone to unsaturated alcohols by H_2 is of great interest in nanocatalysis. In 2010, Jin et al.[38] reported that $Au_{25}(SR)_{18}$ was able to selectively catalyze hydrogenation of the C═O bond of benzalacetone to unsaturated alcohol in toluene/ethanol solvent with 100% chemoselectivity. The Jiang group computationally investigated the mechanism of hydrogenation of benzalacetone by the model $Au_{25}(SCH_3)_{18}$ catalyst.[39] They found that the hydrogenation reaction proceeds via the

DOI: 10.1021/acs.accounts.8b00380
Acc. Chem. Res. 2018, 51, 2793−2802

heterolytic cleavage of H_2 between one staple Au atom of the open facet (Figure 8a) of the $Au_{25}(SR)_{18}$ surface and the

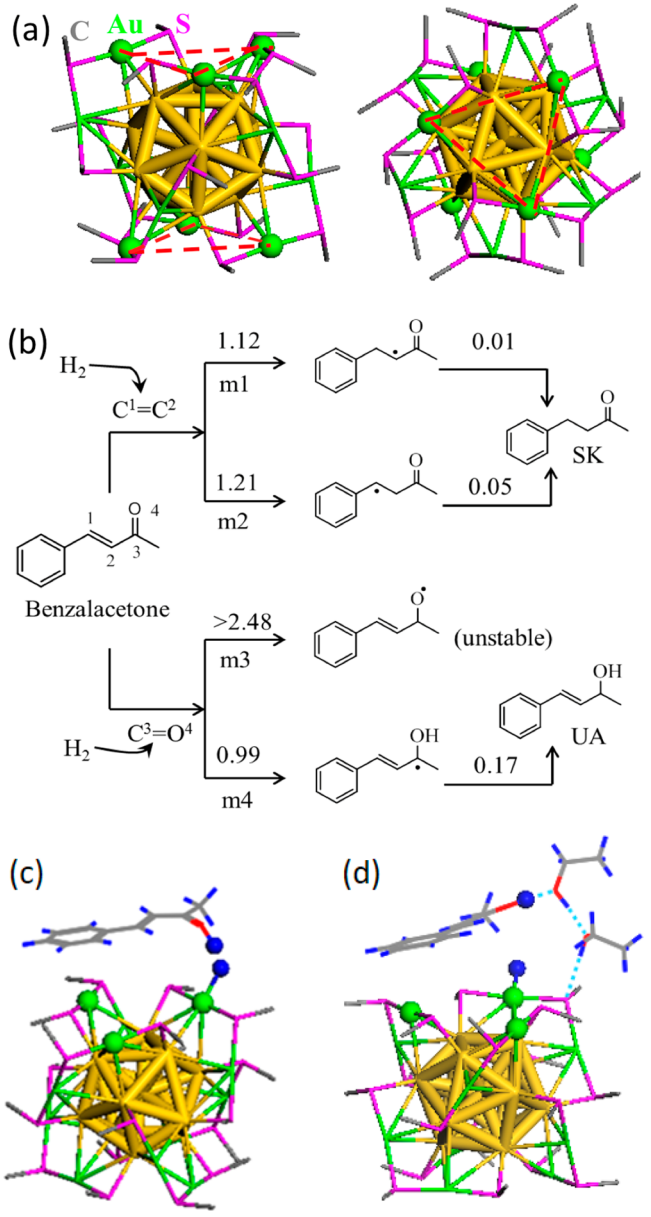

Figure 8. (a) Open facets (dashed triangles) on $Au_{25}(SR)_{18}$: left, side view; right, top view. (b) Hydrogenation pathways of benzalacetone with one H atom of H_2 adding to different positions of benzalacetone, followed by the transfer of the other H atom to the radical intermediate. (c) Transition state for H_2 cleavage via the m4 pathway. (d) The intermediate state of the m4 pathway stabilized by ethanol. Adapted with permission from ref 39. Copyright 2015 American Chemical Society.

carbonyl oxygen (C═O) of the reactant, followed by transfer of H from Au to the carbonyl C to form unsaturated alcohol product (the m4 pathway in Figure 8b; see the transition state in Figure 8c). This pathway has a lower barrier than the other three (m1−m3 in Figure 8b), which explains the experimentally observed selectivity. The presence of ethanol solvent promoted the reaction by stabilizing the intermediate of C═O hydrogenation via hydrogen bond (Figure 8d).

Electrochemical Hydrogen Evolution Reaction (HER)

Doping $Au_{25}(SR)_{18}$ with heteroatoms changes not only the cluster's electronic structure but also the electrocatalytic activity. Recently, a combined experimental-theoretical work by Lee and Jiang[40] showed that doping Pt into $Au_{25}(SR)_{18}$ greatly boosted the cluster's electrocatalytic performance for hydrogen evolution, evidenced by the lower overpotential and higher current compared to pure $Au_{25}(SR)_{18}$ (name shortened as Au_{25}; Figure 9a). The $PtAu_{24}(SR)_{18}$ catalyst (name shortened as $PtAu_{24}$) generated H_2 with turnover frequencies of 4.8 mol H_2 (mol cat)$^{-1}$ s^{-1} in tetrahydrofuran (THF) and 34 mol H_2 (mol cat)$^{-1}$ s^{-1} in water, at a moderate overpotential (η = 0.6 V). This activity is among the best in molecular HER catalysts, even higher than the state-of-the-art Pt/C catalyst (Figure 9b).

The experimental mechanistic studies indicated that at negative reduction potential (<−1.0 V), $PtAu_{24}$ exists primarily in the form of $[PtAu_{24}]^{2-}$, which first reacted with one H^+ to form $[H\text{-}PtAu_{24}]^-$ intermediate, and then reacted with another H^+ to evolve H_2. Our DFT calculations with a simplified solvation model (Figure 9c) revealed that formation of $[H\text{-}PtAu_{24}]^-$ is thermodynamically neutral (step 1). Intriguingly, the H atom directly interacts with the central Pt with a short distance of 1.788 Å. In the second step, the Heyrovsky mechanism (step 2b) is energetically preferred over the Tafel mechanism (step 2a), where the absorbed H in $[H\text{-}PtAu_{24}]^-$ reacts with the solvated proton to produce H_2 and regenerate $PtAu_{24}$. Although $[PtAu_{24}]^{2-}$ and $[Au_{25}]^-$ are isoelectronic, the initial proton absorption is rather endothermic on $[Au_{25}]^-$ (uphill by 0.5 eV), much weaker than on $[PtAu_{24}]^{2-}$ due to the stronger binding affinity of H to Pt. This work clearly demonstrates that doping can be a very powerful way to tune the catalytic properties of $Au_n(SR)_m$ for HER.

Inspired by the H−Pt interaction in the $[H\text{-}PtAu_{24}]^-$ structure, we systematically studied how H interacts with $[Au_{25}(SR)_{18}]^q$ (q = −1, 0, + 1) and monoatom-doped $[M_1Au_{24}(SR)_{18}]^q$ (M = Pt, Pd, Ag, Cu, Hg, Cd, q = −2, −1, 0, + 1) from DFT.[41] It was found that H behaves as a metal and contributes its 1s electron to the superatomic free-electron count. For example, $[PtAu_{24}H_2(SR)_{18}]^0$ was found to be an 8-e system with P-type HOMO and D-type LUMO, being isoelectronic to $[Au_{25}(SR)_{18}]^-$. The metallic nature of H in Au nanoclusters is in contrast with the hydride in Cu or Ag nanoclusters. This can be explained by the fact that H's electronegativity is smaller than Au but larger than Ag or Cu. The calculated Gibbs free energy of H adsorption further confirmed that $PtAu_{24}$ is the most active HER catalyst among those doped Au clusters.

Unlike H in Cu or Ag clusters, no structure of H in ligand-protected gold nanoclusters has been reported. To further explore this opportunity, we investigated H interaction with the diphosphine-protected $Au_{22}(L^8)_6$ cluster (L^8 = 1,8-bis-(diphenylphosphino) octane)[42] which, uniquely, has eight coordinately unsaturated (*cus*) Au atoms (red in Figure 10a). We found from our DFT calculations that $Au_{22}(L^8)_6$ can adsorb up to six H atoms with favorable energetics (Figure 10b), thereby a promising catalyst for hydrogen evolution; Figure 10c shows the first three H atoms adsorbed at the *cus* Au atoms. In fact, H_2 can be activated at the *cus* Au atoms with a moderate barrier and favorable energetics (Figure 10d). Moreover, we found that H behaves as a hydride in the $Au_{22}(L^8)_6$ cluster, in contrast to the metallic H in thiolate-protected Au clusters. This study demonstrated that ligand-protected Au clusters with *cus* Au sites will be the most promising candidates for HER and realizing Au−H nanoclusters and that the behavior

DOI: 10.1021/acs.accounts.8b00380
Acc. Chem. Res. 2018, 51, 2793−2802

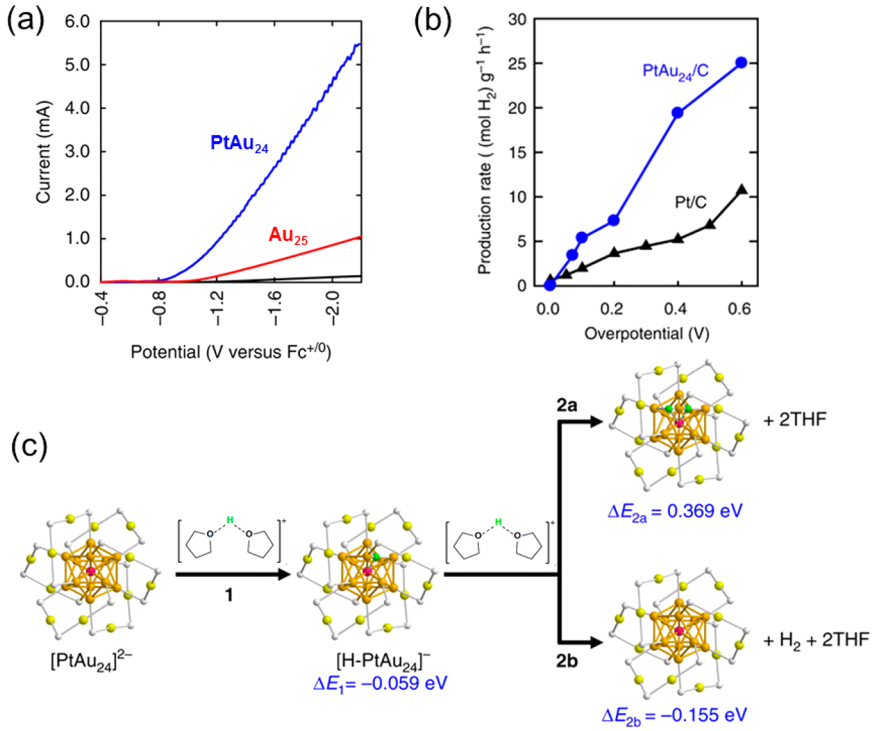

Figure 9. (a) Linear sweep voltammograms of $Au_{25}(SR)_{18}$ and $PtAu_{24}(SR)_{18}$ in THF solution. (b) H_2 production rate on $PtAu_{24}$/C and Pt/C catalyst. (c) DFT-PBE reaction energies for H_2 evolution on $PtAu_{24}$. Adapted with permission from ref 40. Copyright 2017 Nature Publishing Group.

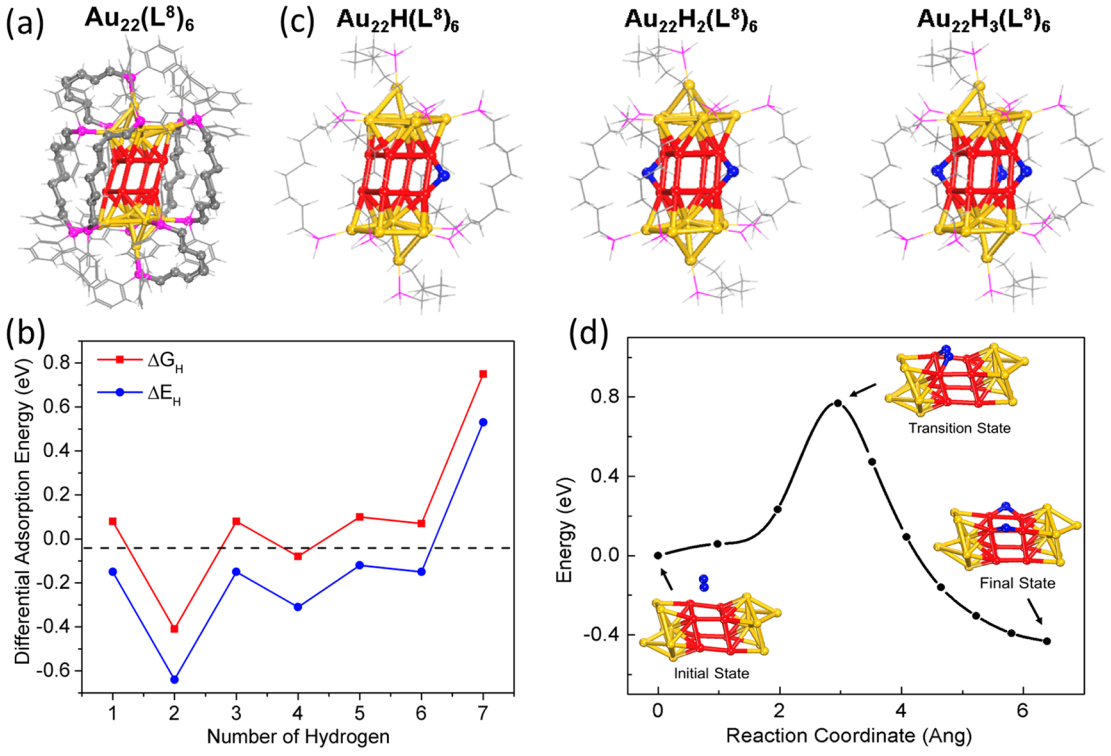

Figure 10. (a) Structure of $Au_{22}(L^8)_6$ cluster; L^8 = 1,8-bis(diphenylphosphino) octane. (b) Differential adsorption energy ΔE_H (blue) and adsorption free energy ΔG_H (red) of H on $Au_{22}(L^8)_6$. (c) Optimized structures of $Au_{22}H_n(L^8)_6$ (n = 1−3). (d) Minimum-energy path of H_2 dissociation on the $Au_{22}(L^8)_6$ cluster; L not shown. Cus Au, red; other Au, yellow; P, magenta; C, gray; H on ligand, light gray; H at the *cus* Au sites, blue. Adapted with permission from ref 42. Copyright 2018 Royal Society of Chemistry.

of H in the clusters depends on the ligands. Interestingly, Tsukuda et al. found hydrogen doping of polymer-protected gold nanoclusters[43] and identified $[Au_9H(PPh_3)_8]^{2+}$ in mass spectrometry and NMR.[44] They further found that hydrogen can be doped into ligand-protected bimetallic nanoclusters to form $(HPdAu_8)^+$ and $(HPdAu_{10})^{3+}$ superatoms.[45]

DOI: 10.1021/acs.accounts.8b00380
Acc. Chem. Res. 2018, 51, 2793−2802

7. CONCLUSIONS AND OUTLOOK

DFT-based first-principles studies have provided important insights into the fundamental issues in atomically precise metal nanoclusters, including the interfacial bonding, energetics, electronic structure, optical properties, and catalytic mechanisms. The interfacial structures on gold are ligand-dependent, closely related to the metal core geometry and surface facets as well as the coordination preferences for different ligands. For thiolates, we found a surface-sensitive choice of staple vs bridging motifs. The emerging alkynyls and bulky *N*-heterocyclic carbenes were found to form stronger interfaces than thiolates and phosphines. The similarity and difference between alkynyls and thiolates have provided many new insights. Ligands could also change the energy landscape of a cluster of the same composition by affecting the geometric construction of the core via the ligand−ligand interaction. Time-dependent DFT calculations are useful in understanding the optical-absorption spectral, which are sensitive to changes in geometry and electronic structure introduced by doping. Spin−orbit coupling needs to be included to accurately describe the orbital level and reproduce the optical-absorption spectra of gold nanoclusters. Moreover, atomically precise nanoclusters offer great opportunities in understanding nanocatalysis, by allowing theory to identify the active sites and predict the selectivity.

Despite the great advances, many important questions remain to be addressed. First of all, a first-principles understanding of the formation-and-growth mechanism, or "the origin of the species", is still missing. This topic is ready to be tackled via a multiscale modeling approach in collaboration with in situ experimental characterization. This will be key to making the synthesis of the clusters a science rather than an art. Second, the NHC ligands are attractive yet no structure of such cluster has been reported; a breakthrough in this area is needed. Third, the parallelism between thiolate-gold and alkynyl-gold interfaces suggests a potential cross-fertilization between the two universes, e.g., using a mixture of thiolate and alkynyl ligands in synthesis; and the possibility of synthesizing $Au_{25}(CCR)_{18}$ and $Au_{38}(CCR)_{24}$. Fourth, the overwhelming majority of DFT studies of atomically gold clusters do not include spin−orbit coupling (SOC), since it greatly increases the computational cost; it remains to be explored how SOC affects the electronic structures of the great many other gold clusters, including the doped and larger ones. Last but not least, the predicted high reactivity of diphosphine-protected $Au_{22}(L^8)_6$ cluster for electrocatalytic H_2 evolution needs future experimental verification and, more importantly, the idea of producing *cus* metal sites in atomically precise clusters should be pursued, as they are most promising for catalysis.

AUTHOR INFORMATION

Corresponding Author

*E-mail: djiang@ucr.edu.

ORCID

Qing Tang: 0000-0003-0805-7506
Victor Fung: 0000-0002-3347-6983
De-en Jiang: 0000-0001-5167-0731

Notes

The authors declare no competing financial interest.

Biographies

Qing Tang is a chemistry professor at Chongqing University. She conducted her postdoctoral research with Prof. De-en Jiang at University of California Riverside (UCR) after receiving her Ph.D. from Nankai University. Her research interests are theoretical studies of low-dimensional nanomaterials and electrocatalysis.

Guoxiang Hu received her B.S. in chemistry from University of Science and Technology of China. She recently completed her Ph.D. research on first-principles studies of surface chemistry and catalysis with Prof. Jiang at UCR.

Victor Fung earned his B.A. in chemistry at Cornell University and is currently a Ph.D. candidate working on computational catalysis in the Jiang group at UCR.

De-en Jiang is an associate professor of chemistry at UCR. He received his B.S. and M.S. from Peking University and Ph.D. from UCLA. He was a staff scientist at Oak Ridge National Laboratory before joining UCR in 2014. His research focuses on computational materials chemistry and nanoscience for energy and the environment.

ACKNOWLEDGMENTS

This work was sponsored by the U.S. Department of Energy, Office of Science, Office of Basic Energy Sciences, Chemical Sciences, Geosciences, and Biosciences Division and University of California Riverside. This research used resources of the National Energy Research Scientific Computing Center, a DOE Office of Science User Facility supported by the Office of Science of the U.S. Department of Energy under Contract No. DE-AC02-05CH11231.

REFERENCES

(1) Jin, R.; Zeng, C.; Zhou, M.; Chen, Y. Atomically Precise Colloidal Metal Nanoclusters and Nanoparticles: Fundamentals and Opportunities. *Chem. Rev.* **2016**, *116*, 10346−10413.

(2) Dhayal, R. S.; van Zyl, W. E.; Liu, C. W. Polyhydrido Copper Clusters: Synthetic Advances, Structural Diversity, and Nanocluster-to-Nanoparticle Conversion. *Acc. Chem. Res.* **2016**, *49*, 86−95.

(3) Yao, Q. F.; Chen, T. K.; Yuan, X.; Xie, J. P. Toward Total Synthesis of Thiolate-Protected Metal Nanoclusters. *Acc. Chem. Res.* **2018**, *51*, 1338−1348.

(4) Lei, Z.; Wan, X. K.; Yuan, S. F.; Wang, J. Q.; Wang, Q. M. Alkynyl-protected gold and gold-silver nanoclusters. *Dalton Trans.* **2017**, *46*, 3427−3434.

(5) Zhukhovitskiy, A. V.; MacLeod, M. J.; Johnson, J. A. Carbene Ligands in Surface Chemistry: From Stabilization of Discrete Elemental Allotropes to Modification of Nanoscale and Bulk Substrates. *Chem. Rev.* **2015**, *115*, 11503−11532.

(6) Jiang, D.-E. The expanding universe of thiolated gold nanoclusters and beyond. *Nanoscale* **2013**, *5*, 7149−7160.

(7) Pei, Y.; Zeng, X. C. Investigating the structural evolution of thiolate protected gold clusters from first-principles. *Nanoscale* **2012**, *4*, 4054−4072.

(8) Walter, M.; Akola, J.; Lopez-Acevedo, O.; Jadzinsky, P. D.; Calero, G.; Ackerson, C. J.; Whetten, R. L.; Groenbeck, H.; Hakkinen, H. A unified view of ligand-protected gold clusters as superatom complexes. *Proc. Natl. Acad. Sci. U. S. A.* **2008**, *105*, 9157−9162.

(9) Maksymovych, P.; Sorescu, D. C.; Yates, J. T., Jr. Gold-adatom-mediated bonding in self-assembled short-chain alkanethiolate species on the Au(111) surface. *Phys. Rev. Lett.* **2006**, *97*, 146103.

(10) Jadzinsky, P. D.; Calero, G.; Ackerson, C. J.; Bushnell, D. A.; Kornberg, R. D. Structure of a thiol monolayer-protected gold nanoparticle at 1.1 angstrom resolution. *Science* **2007**, *318*, 430−433.

(11) Zeng, C.; Liu, C.; Chen, Y.; Rosi, N. L.; Jin, R. Atomic structure of self-assembled monolayer of thiolates on a tetragonal Au_{92} nanocrystal. *J. Am. Chem. Soc.* **2016**, *138*, 8710−8713.

DOI: 10.1021/acs.accounts.8b00380
Acc. Chem. Res. 2018, 51, 2793−2802

(12) Hu, G.; Jin, R.; Jiang, D.-E. Beyond the staple motif: a new order at the thiolate−gold interface. *Nanoscale* **2016**, *8*, 20103−20110.
(13) Maity, P.; Tsunoyama, H.; Yamauchi, M.; Xie, S.; Tsukuda, T. Organogold clusters protected by phenylacetylene. *J. Am. Chem. Soc.* **2011**, *133*, 20123−20125.
(14) Tang, Q.; Jiang, D.-E. Insights into the PhC≡C/Au Interface. *J. Phys. Chem. C* **2015**, *119*, 10804−10810.
(15) Wang, Y.; Wan, X.-K.; Ren, L.; Su, H.; Li, G.; Malola, S.; Lin, S.; Tang, Z.; Häkkinen, H.; Teo, B. K.; et al. Atomically precise alkynyl-protected metal nanoclusters as a model catalyst: Observation of promoting effect of surface ligands on catalysis by metal nanoparticles. *J. Am. Chem. Soc.* **2016**, *138*, 3278−3281.
(16) Wang, Y.; Su, H.; Xu, C.; Li, G.; Gell, L.; Lin, S.; Tang, Z.; Häkkinen, H.; Zheng, N. An intermetallic $Au_{24}Ag_{20}$ superatom nanocluster stabilized by labile ligands. *J. Am. Chem. Soc.* **2015**, *137*, 4324−4327.
(17) Wan, X.-K.; Guan, Z.-J.; Wang, Q.-M. Homoleptic Alkynyl-Protected Gold Nanoclusters: $Au_{44}(PhCC)_{28}$ and $Au_{36}(PhCC)_{24}$. *Angew. Chem.* **2017**, *129*, 11652−11655.
(18) Lei, Z.; Li, J.-J.; Wan, X.-K.; Zhang, W.-H.; Wang, Q.-M. Isolation and Total Structure Determination of an All-Alkynyl-Protected Gold Nanocluster Au_{144}. *Angew. Chem., Int. Ed.* **2018**, *57*, 8639−8643.
(19) Crudden, C. M.; Horton, J. H.; Narouz, M. R.; Li, Z.; Smith, C. A.; Munro, K.; Baddeley, C. J.; Larrea, C. R.; Drevniok, B.; Thanabalasingam, B.; et al. Simple direct formation of self-assembled N-heterocyclic carbene monolayers on gold and their application in biosensing. *Nat. Commun.* **2016**, *7*, 12654.
(20) Wang, G.; Rühling, A.; Amirjalayer, S.; Knor, M.; Ernst, J. B.; Richter, C.; Gao, H.-J.; Timmer, A.; Gao, H.-Y.; Doltsinis, N. L.; et al. Ballbot-type motion of N-heterocyclic carbenes on gold surfaces. *Nat. Chem.* **2017**, *9*, 152−156.
(21) Tang, Q.; Jiang, D.-E. Comprehensive View of the Ligand−Gold Interface from First Principles. *Chem. Mater.* **2017**, *29*, 6908−6915.
(22) Jiang, L.; Zhang, B.; Médard, G.; Seitsonen, A. P.; Haag, F.; Allegretti, F.; Reichert, J.; Kuster, B.; Barth, J. V.; Papageorgiou, A. C. N-heterocyclic carbenes on close-packed coinage metal surfaces: bis-carbene metal adatom bonding scheme of monolayer films on Au, Ag and Cu. *Chem. Sci.* **2017**, *8*, 8301−8308.
(23) Larrea, C. R.; Baddeley, C. J.; Narouz, M. R.; Mosey, N. J.; Horton, J. H.; Crudden, C. M. N-Heterocyclic Carbene Self-assembled Monolayers on Copper and Gold: Dramatic Effect of Wingtip Groups on Binding, Orientation and Assembly. *ChemPhysChem* **2017**, *18*, 3536−3539.
(24) Pei, Y.; Pal, R.; Liu, C.; Gao, Y.; Zhang, Z.; Zeng, X. C. Interlocked catenane-like structure predicted in $Au_{24}(SR)_{20}$Implication to structural evolution of thiolated gold clusters from homoleptic gold (I) thiolates to core-stacked nanoparticles. *J. Am. Chem. Soc.* **2012**, *134*, 3015−3024.
(25) Das, A.; Li, T.; Li, G.; Nobusada, K.; Zeng, C.; Rosi, N. L.; Jin, R. Crystal structure and electronic properties of a thiolate-protected Au_{24} nanocluster. *Nanoscale* **2014**, *6*, 6458−6462.
(26) Tang, Q.; Ouyang, R.; Tian, Z.; Jiang, D.-E. The ligand effect on the isomer stability of $Au_{24}(SR)_{20}$ clusters. *Nanoscale* **2015**, *7*, 2225−2229.
(27) Chen, Y.; Liu, C.; Tang, Q.; Zeng, C.; Higaki, T.; Das, A.; Jiang, D.-E.; Rosi, N. L.; Jin, R. Isomerism in $Au_{28}(SR)_{20}$ nanocluster and stable structures. *J. Am. Chem. Soc.* **2016**, *138*, 1482−1485.
(28) Tian, S.; Li, Y.-Z.; Li, M.-B.; Yuan, J.; Yang, J.; Wu, Z.; Jin, R. Structural isomerism in gold nanoparticles revealed by X-ray crystallography. *Nat. Commun.* **2015**, *6*, 8667.
(29) Jiang, D.-E.; Kühn, M.; Tang, Q.; Weigend, F. Superatomic orbitals under spin−orbit coupling. *J. Phys. Chem. Lett.* **2014**, *5*, 3286−3289.
(30) Zhu, M.; Aikens, C. M.; Hollander, F. J.; Schatz, G. C.; Jin, R. Correlating the crystal structure of a thiol-protected Au_{25} cluster and optical properties. *J. Am. Chem. Soc.* **2008**, *130*, 5883−5885.
(31) Devadas, M. S.; Bairu, S.; Qian, H.; Sinn, E.; Jin, R.; Ramakrishna, G. Temperature-dependent optical absorption properties of monolayer-protected Au_{25} and Au_{38} clusters. *J. Phys. Chem. Lett.* **2011**, *2*, 2752−2758.
(32) Kwak, K.; Tang, Q.; Kim, M.; Jiang, D.-E.; Lee, D. Interconversion between superatomic 6-electron and 8-electron configurations of $M@Au_{24}(SR)_{18}$ clusters (M= Pd, Pt). *J. Am. Chem. Soc.* **2015**, *137*, 10833−10840.
(33) Jiang, D.-E.; Dai, S. From superatomic $Au_{25}(SR)_{18}^{-}$ to superatomic $M@Au_{24}(SR)_{18}^{q}$ core−shell clusters. *Inorg. Chem.* **2009**, *48*, 2720−2722.
(34) Negishi, Y.; Kurashige, W.; Niihori, Y.; Iwasa, T.; Nobusada, K. Isolation, structure, and stability of a dodecanethiolate-protected Pd_1Au_{24} cluster. *Phys. Chem. Chem. Phys.* **2010**, *12*, 6219−6225.
(35) Qian, H.; Jiang, D.-E.; Li, G.; Gayathri, C.; Das, A.; Gil, R. R.; Jin, R. Monoplatinum doping of gold nanoclusters and catalytic application. *J. Am. Chem. Soc.* **2012**, *134*, 16159−16162.
(36) Tian, S.; Liao, L.; Yuan, J.; Yao, C.; Chen, J.; Yang, J.; Wu, Z. Structures and magnetism of mono-palladium and mono-platinum doped $Au_{25}(PET)_{18}$ nanoclusters. *Chem. Commun.* **2016**, *52*, 9873−9876.
(37) Kim, M.; Tang, Q.; Kumar, A. V. N.; Kwak, K.; Choi, W.; Jiang, D.-E.; Lee, D. Dopant-Dependent Electronic Structures Observed for $M_2Au_{36}(SC_6H_{13})_{24}$ Clusters (M= Pt, Pd). *J. Phys. Chem. Lett.* **2018**, *9*, 982−989.
(38) Zhu, Y.; Qian, H.; Drake, B. A.; Jin, R. Atomically Precise $Au_{25}(SR)_{18}$ Nanoparticles as Catalysts for the Selective Hydrogenation of α,β-Unsaturated Ketones and Aldehydes. *Angew. Chem.* **2010**, *122*, 1317−1320.
(39) Ouyang, R.; Jiang, D.-E. Understanding selective hydrogenation of α,β-unsaturated ketones to unsaturated alcohols on the $Au_{25}(SR)_{18}$ cluster. *ACS Catal.* **2015**, *5*, 6624−6629.
(40) Kwak, K.; Choi, W.; Tang, Q.; Kim, M.; Lee, Y.; Jiang, D.-E.; Lee, D. A molecule-like $PtAu_{24}(SC_6H_{13})_{18}$ nanocluster as an electrocatalyst for hydrogen production. *Nat. Commun.* **2017**, *8*, 14723.
(41) Hu, G.; Tang, Q.; Lee, D.; Wu, Z.; Jiang, D.-E. Metallic Hydrogen in Atomically Precise Gold Nanoclusters. *Chem. Mater.* **2017**, *29*, 4840−4847.
(42) Hu, G. X.; Wu, Z. L.; Jiang, D. E. Stronger-than-Pt hydrogen adsorption in a Au_{22} nanocluster for the hydrogen evolution reaction. *J. Mater. Chem. A* **2018**, *6*, 7532−7537.
(43) Ishida, R.; Hayashi, S.; Yamazoe, S.; Kato, K.; Tsukuda, T. Hydrogen-Mediated Electron Doping of Gold Clusters As Revealed by In Situ X-ray and UV-vis Absorption Spectroscopy. *J. Phys. Chem. Lett.* **2017**, *8*, 2368−2372.
(44) Takano, S.; Hirai, H.; Muramatsu, S.; Tsukuda, T. Hydride-Doped Gold Superatom $(Au_9H)^{2+}$: Synthesis, Structure, and Transformation. *J. Am. Chem. Soc.* **2018**, *140*, 8380−8383.
(45) Takano, S.; Hirai, H.; Muramatsu, S.; Tsukuda, T. Hydride-Mediated Controlled Growth of a Bimetallic $(Pd@Au_8)^{2+}$ Superatom to a Hydride-Doped $(HPd@Au_{10})^{3+}$ Superatom. *J. Am. Chem. Soc.* **2018**, *140*, 12314−12317.

DOI: 10.1021/acs.accounts.8b00380
Acc. Chem. Res. 2018, 51, 2793−2802